NANO LETTERS

Letter

pubs.acs.org/NanoLett

Graphene-Enhanced Brillouin Optomechanical Microresonator for Ultrasensitive Gas Detection

Baicheng Yao,[*,†,‡,§] Caibin Yu,[†] Yu Wu,[†] Shu-Wei Huang,[‡] Han Wu,[†] Yuan Gong,[†,∥] Yuanfu Chen,[⊥] Yanrong Li,[⊥] Chee Wei Wong,[‡] Xudong Fan,[∥] and Yunjiang Rao[*,†]

[†]Key Laboratory of Optical Fiber Sensing and Communications (Education Ministry of China), University of Electronic Science and Technology of China, Chengdu 610054, China

[‡]Fang Lu Mesoscopic Optics and Quantum Electronics Laboratory, University of California, Los Angeles, California 90095, United States

[§]Cambridge Graphene Center, University of Cambridge, Cambridge CB3 0FA, United Kingdom

[∥]Department of Biomedical Engineering, University of Michigan, Ann Arbor, Michigan 48109, United States

[⊥]State Key Laboratory of Electronic Thin Films and Integrated Devices, University of Electronic Science and Technology of China, Chengdu 610054, China

S *Supporting Information*

ABSTRACT: Chemical sensing is one of the most important applications of nanoscience, whose ultimate aim is to seek higher sensitivity. In recent years, graphene with intriguing quantum properties has spurred dramatic advances ranging from materials science to optoelectronics and mechanics, showing its potential to realize individual molecule solid-state sensors. However, for optical sensing the single atom thickness of graphene greatly limits the light-graphene interactions, bottlenecking their performances. Here we demonstrate a novel approach based on the forward phase-matched Brillouin optomechanics in a graphene inner-deposited high Q ($>2 \times 10^6$) microfluidic resonator, expanding the "electron−photon" interaction in conventional graphene optical devices to the "electron−phonon−photon" process. The molecular adsorption induced surface elastic modulation in graphene enables the Brillouin optomechanical modes (mechanical $Q \approx 43{,}670$) extremely sensitive (200 kHz/ppm) in ammonia gas detection, achieving a noise equivalent detection limit down to 1 ppb and an unprecedented dynamic range over five orders-of-magnitude with fast response. This work provides a new platform for the researches of graphene-based optomechanics, nanophotonics, and optical sensing.

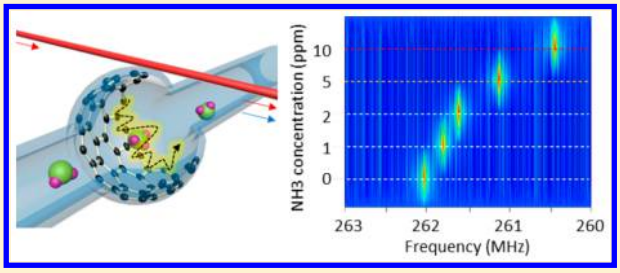

KEYWORDS: *Graphene, Brillouin optomechnics, whispering gallery mode microresonator, fiber interrogated optics, ultrasensitive gas detection*

Since discovered in 2004,[1] graphene has brought unprecedented breakthroughs across the domains of optoelectronics, mechanics, and thermal transport, driven by its quasiparticle Dirac Fermions obeying a linear dispersion in the individual quanta level.[2] Accordingly, graphene shows the unique potential to realize broadband optoelectronic modulators[3−5], ultrafast light sources/detectors,[6,7] optomechanical devices,[8−11] and highly sensitive bio and chemical sensors.[12−14] Significantly, graphene enables gas detection with single molecule sensitivity on solid-state gas detectors, as gas adsorption on graphene changes the local carrier concentration.[15−17] In contrast, limited by the graphene−light interaction efficiency, most graphene-based optical gas sensors have a maximum sensitivity of sub part per million (ppm),[18] showing no significant advantages over existing techniques. To breakthrough this limit and realize a graphene-based optical sensor with individual molecule sensitivity, both the sensing mechanism and the associated technique need to be further explored.

Here we report a graphene based optomechanical microresonator and demonstrate its potential for ultrasensitive gas detection. A layer of nanometer-thick reduced graphene oxide (rGO) film is uniformly incorporated in a whispering gallery mode (WGM) bottle-shaped cavity with optical Q-factor $>2 \times 10^6$, enhancing the forward phase-matched stimulated Brillouin scattering (F-SBS) resonance with a mechanical Q-factor ≈43 670 for a selected resonant mode at 262 MHz. In previous reports, optomechanics in a WGM cavity has shown exceptionally ultralow dissipation and ultrahigh phase correlation[19] with great potential in optofluidics[20] and light storage.[21] However, to apply the F-SBS to detect gas is still elusive. In this

Received: May 24, 2017
Revised: July 12, 2017
Published: July 14, 2017

DOI: 10.1021/acs.nanolett.7b02176
Nano Lett. 2017, 17, 4996−5002

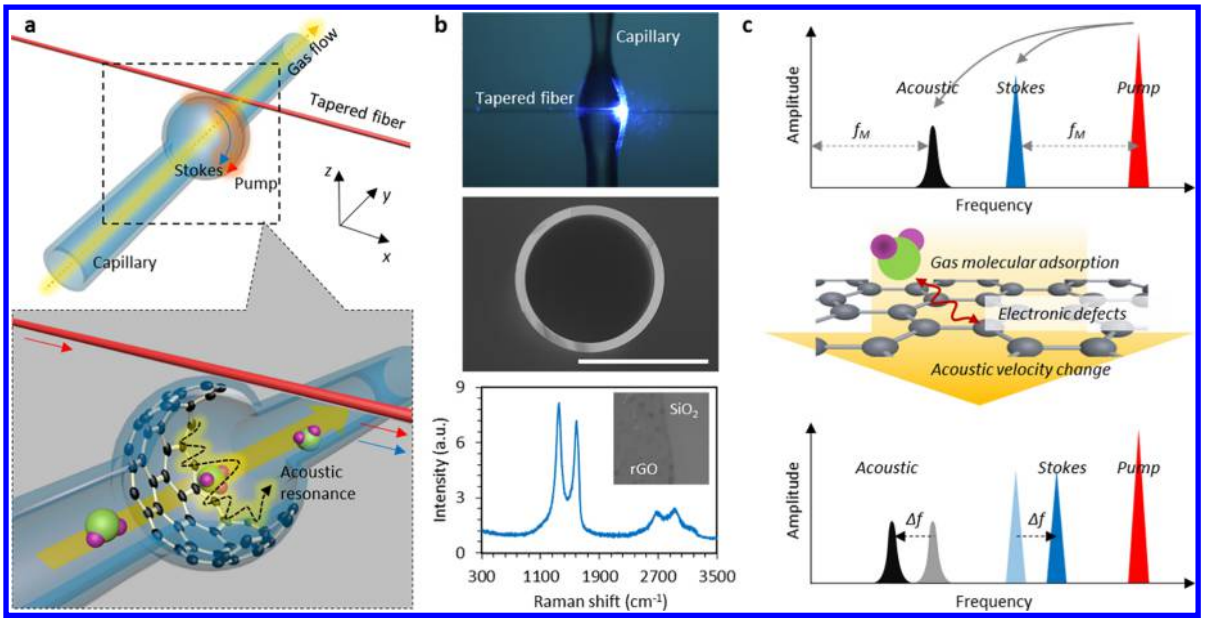

Figure 1. Conceptual design and implementation of the graphene enhanced Brillouin optomechanics. (a) Schematic of the GBMR. An rGO film is incorporated in a bottle-shaped silica capillary resonator and a pump laser is coupled in using a tapered fiber. In this resonator, the pump mode (red arrow) generates the Stokes mode (blue arrow) and the acoustic mechanical resonance mode (black arrow). (b) From top to bottom: top view micrograph, cross-sectional SEM picture of the GBMR and Raman spectrum of the rGO film. In this panel, the bars show 100 μm. Inset: scanning electron micrograph of the rGO film deposited on the silica wall. The bar shows 100 μm. (c) Optical process of the F-SBS generated in the GBMR and how it is modulated by the gas molecules attached to the rGO surface.

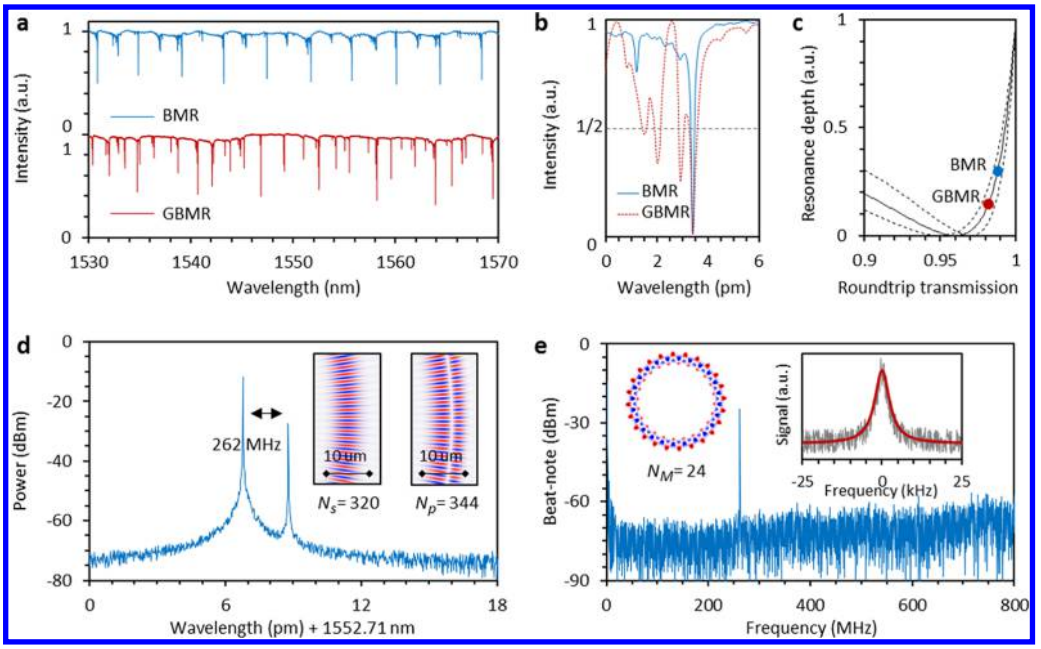

Figure 2. Generation of the optomechanical resonances in the multimode WGM cavity. (a) Transmission spectra of the bottle-shaped cavity, before (BMR, blue curve) and after rGO deposition (GBMR, red curve). (b) Typical optical resonance dips of the BMR (blue) and the GBMR (red). In (a,b), transmissions are linearly normalized. (c) Correlation of the roundtrip transmissions and the tapered fiber transmissions. Here the curves show the calculated results with coupling rates at 3%, 4% (solid), and 5%, respectively. Blue and red dots show the measured results of the BMR and the GBMR separately. (d) Measured spectrum of the generated Stokes line located at 1557.719 nm, when pump wavelength is fixed at 1552.717 nm. Inset: simulations of the longitudinal order of the pump mode and the Stokes mode at 344 and 320 respectively. (e) Beat note of the pump and the Stokes, showing mechanical mode frequency 262 MHz. Inset: simulation of mechanical mode distribution with order of 24. Inset: spectrum line width of 6 kHz, estimated by a Lorentzian fitting.

work, the in-cavity deposited rGO enhances the high order WGM modes and modulates the F-SBS based optomechanical resonances based on gas molecule adsorption,[22,23] expanding the "electron−photon" interaction in conventional graphene-based photonic sensors to the "electron−phonon−photon" interaction. Measured via RF spectroscopy with single Hz resolution, the fiber-coupled compact all-optical sensor based on the graphene enhanced Brillouin optomechanical micro-resonance approaches a detection limit down to 1 part per billion (ppb) and a wide dynamic range over 5 orders of

DOI: 10.1021/acs.nanolett.7b02176
Nano Lett. 2017, 17, 4996−5002

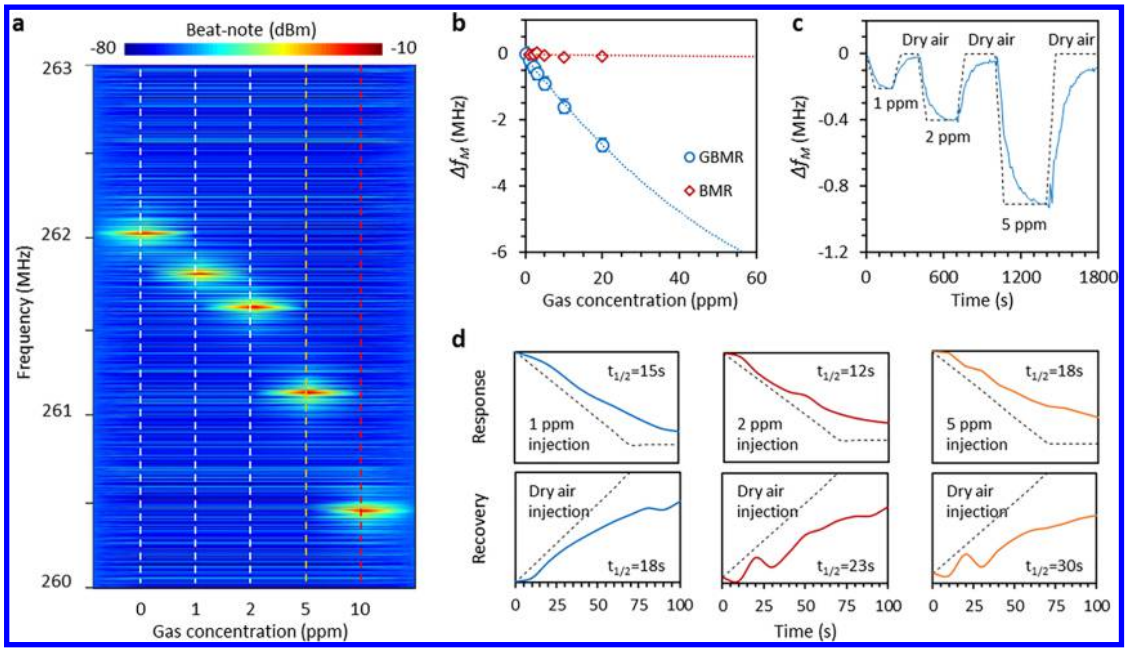

Figure 3. NH_3 gas detection. (a) Colored map of the beat note spectra varies with the NH_3 gas concentration. When NH_3 gas concentration increases from 0 to 10 ppm, f_M decreases from 262.0 to 260.4 MHz. (b) Correlation of the NH_3 gas concentration and the shift (Δf_M). Here the blue circles show the measured results from the GBMR whereas the red diamonds show the measured results from the BMR. (c) Regeneration of the GBMR sensor in NH_3 sensing. (d) Response and recovery time of the GBMR sensor.

magnitude (1 ppb to 370 ppm) for ammonia gas, an important chemical compound in industrial, environmental, and safety monitoring.

Figure 1a demonstrates the schematic design of the graphene enhanced Brillouin microresonator (GBMR). A microscale bottle-shaped capillary serves as both the optomechanical cavity and the gas fluidic channel. A tapered fiber with diameter of ≈1 μm is applied to launch and collect optical modes from the resonator along the x-axis, while gas molecules are injected into the cell along the y-axis. By using the fiber-splicer based arc discharge method, we fabricated the bottle-shaped microresonator (BMR) from a silica capillary (inner diameter 83 μm, outer diameter 100 μm), the diameter of the bottle-shaped section is 119 μm with silica wall thickness 8 μm. A layer of rGO film is deposited on the inner wall of the BMR via aqueous reduction technique. The thickness of the rGO film is estimated to be 3−5 nm.[24,25] Figure 1b shows the micrographs of the GBMR and Raman spectrum of the rGO deposition. Driven by 1550 nm laser excitation, insertion loss of the GBMR is ≈5 dB. The inset of the Raman spectrum shows a scanning electron micrograph of the thin rGO film, verifying its uniformity. Fabrication process is detailed in Supplementary Figure S3.

The sensing mechanism of the GBMR for gas detection is shown in Figure 1c. Different from single-mode fibers predominantly supporting 11 GHz backward SBS, WGM cavities allow F-SBS ranging from tens of megahertz to tens of gigahertz, when the optical modes and the acoustic mode satisfy the energy and momentum conservation, that is, $f_p = f_s + f_M$, $\boldsymbol{k}_p = \boldsymbol{k}_s + \boldsymbol{k}_M$. Here subscript p, s, and M denote the pump mode, the Stokes mode, and the acoustic mechanical resonance mode, respectively. Referring to acoustic dispersion $f_M = v_A|\boldsymbol{k}_M|$ and optical dispersion $|\boldsymbol{k}_{s,p}| = 2\pi f_{s,p} n_{s,p}/c$, we can describe the phase-matching condition as

$$f_s = \frac{c - 2\pi v_A n_p}{c - 2\pi v_A n_s} f_p \quad (1)$$

where v_A is the effective in-cavity acoustic velocity, and n_p and n_s are the effective refractive indexes of the pump mode and the Stokes mode, respectively ($n_p > n_s$). c is the light velocity in vacuum. To satisfy eq 1, n_s should be smaller than n_p, meaning that the pump mode and the Stokes mode should be in different orders. For a phase-matched F-SBS in the optomechanical cavity, once the pump frequency is fixed the resonant Stokes frequency is determined by v_A, which is proportional to the square of the elastic modulus in the microresonator. The gas molecules adsorbed on the surface of graphene, causing local lattice strain to change,[22] which subsequently modifies the value of v_A and hence the phase matching condition. Theoretical analysis is in Supplementary Section S1. As a result, the number of gas molecules on the rGO surface, which correlates with the gas concentration in the sensing cell, can be accurately detected using an RF analyzer that monitors the optical heterodyne beat collected from the tapered fiber.

Figure 2a plots the transmissions of the BMR versus a GBMR, in range of 1530 to 1570 nm. Determined by its geometry, the GBMR designed for tunable F-SBS excitation exhibits many high-order mode resonances. Moreover, due to the rGO film (a high index material) deposition, high-order modes in the GBMR are dramatically enhanced compared to the BMR. Such an optical enhancement is directly reflected in the free spectrum ranges (FSRs)[26]. In the BMR, the FSR of the fundamental mode is ≈4.4 nm, while the FSR of the fundamental mode in the GBMR is ≈5.7 nm, also suggesting the effective index of the GBMR is smaller than the BMR.

Figure 2b expands on the transmission and compares the resonant dips of the BMR and the GBMR (here their extinction ratios are normalized, the resonances are selected around 1552 nm: Λ_{BMR} = 1551.75 nm, Λ_{GBMR} = 1552.53 nm). The optical Q-factor of the fundamental (TM_{01}) mode of the BMR here is ≈8×10^6, which is typical for a silica bottle-shaped cavity. The WGM does not have much electrical field on the inner surface,

DOI: 10.1021/acs.nanolett.7b02176
Nano Lett. 2017, 17, 4996−5002

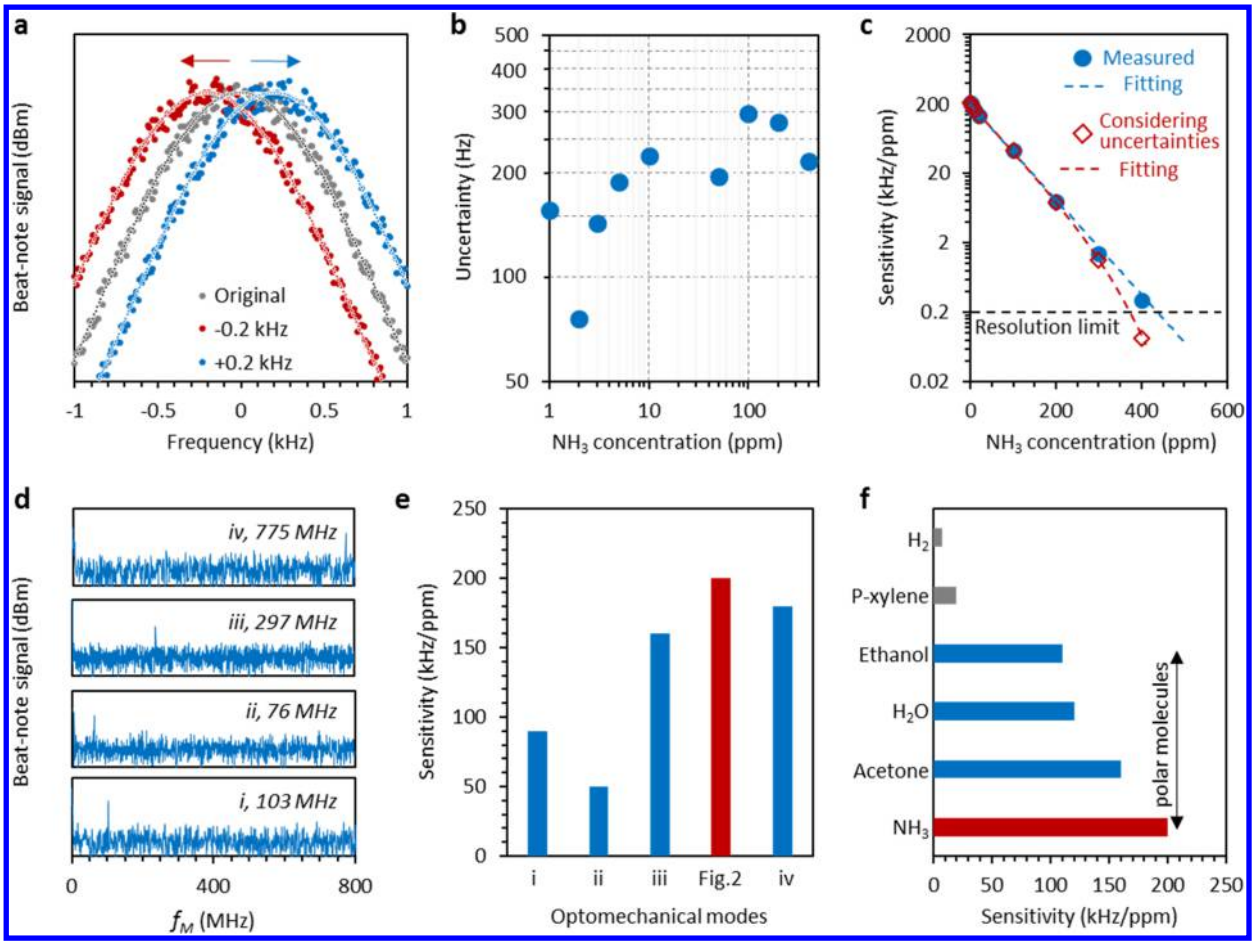

Figure 4. Brillouin and acoustic optomechanics sensing performance. (a) Zoom-in of the beat note when shifting ±200 Hz, such a spectral shift is well distinguishable. (b) Allen deviation plot of f_M, during gas detection. Average instability of the F-SBS in the GBMR is below 200 Hz. Results in (a,b) provide a potential estimate of the detection limit for the sensor. (c) Sensitivity (blue dots) decreases with NH_3 gas concentration, providing an estimate of the dynamic range of the sensor. For higher gas concentration, influence of the uncertainty becomes more critical (red diamonds). (d) Other generated mechanical modes, by tuning f_p, mode samples i to iv are demonstrated, each of these oscillations obeys the forward Brillouin phase matching condition. (e) Sensitivities of the mechanical mode samples, varying from 50 to 200 kHz/ppm. Here the red highlighted one is the selected mode oscillating at 262 MHz, as shown in Figure 2. (f) Specificity of the GBMR gas sensor, shows good selectivity to polar molecules.

so the rGO absorption induced *Q*-factor reduction is relatively small, maintaining its maximum loaded *Q*-factor ≈2 × 10^6 (intrinsic $Q \approx 2.25 \times 10^6$), for the fundamental mode. High-order resonant modes close to the fundamental mode are observed, where the mode-to-mode spectral distance ranges from several megahertz to hundreds of megahertz. We note that the *Q*-factors of different resonances are varied; typically, a resonance of higher order mode or stronger scattering has lower *Q*-factor. More details are shown in Supplementary Figure S4. Figure 2c shows the "round trip transmission−resonance depth" correlation[27]. In our measurements, the fiber-to-cavity coupling rate is ≈4% and the BMR cavity is in the overcoupled regime. Because of the graphene induced loss, the GBMR is closer to the critical coupling point.

By tuning pump wavelength to 1552.717 nm (power launched in the GBMR P_p = 400 μW, higher than the F-SBS threshold $P_{th} \approx 250$ μW), we excite an optomechanical mode with f_M = 262 MHz in the GBMR (in air, room temperature). Figure 2d demonstrates the pump and the Stokes line in a high-resolution optical spectrum analyzer (OSA). The generated Stokes line is located at 1552.719 nm, an ≈2 pm offset from the pump. In addition, there is no anti-Stokes line or cascaded harmonics, verifying that only F-SBS contributes in this nonlinear process. With finite element computation, we also illustrate the simulated mode distributions of the pump and Stokes mode in the insets with the longitudinal mode order at the pump frequency N_p = 344, and N_s = 320. In this case, we also have a longitudinal mode order of the acoustic mechanical resonance N_M = 24. Correspondingly, Figure 2e shows the pump-Stokes beat note in a RF spectrum analyzer. The location of the mechanical resonance is at 262 MHz and its signal-to-noise ratio is higher than 30 dB. The insets of Figure 2e illustrate the simulated mechanical mode distribution in the cavity and the measured mechanical line width of the beat note Δf_M of ≈6 kHz, estimating its mechanical $Q \approx 43\,670$. Such a narrow line width is determined by both the phase matching of the F-SBS and the lasing excitation process.

Following the observations of the Brillouin and acoustic mechanical scattering, an ammonia gas (NH_3) sample is introduced into the capillary gas cell by using a microinjection system with concentration ranging from 1 to 10 ppm and with a fixed flow rate of 1 nL/min. The volume of the GBMR for gas filling is ≈0.7 nL. That means under typical atmospheric pressure and room temperature 1 ppm of NH_3 gas in this GBMR has ≈1.84 × 10^7 NH_3 molecules. Experimental setup

DOI: 10.1021/acs.nanolett.7b02176
Nano Lett. 2017, 17, 4996−5002

and gas sample preparation are shown in Supplementary Figure S5 and Figure S6.

Figure 3a maps the measured RF spectra in NH_3 detection. When the GBMR cell filled with air, the beat note peak is located at 262.0 MHz originally. Perturbed by NH_3 injection with concentrations of 1, 2, 5, and 10 ppm, the beat note peak shifts to 261.8, 261.6, 261.1, and 260.4 MHz, respectively. It reflects that the mechanical resonance responds effectively to the gas molecule adsorption on the rGO film. We also note that such a spectral shift does not change the mode-to-mode phase matching and the mechanical mode order is kept at 24. Hence, during the gas sensing process the mechanical Q remains almost the same. Figure 3b demonstrates the NH_3 concentration versus Δf correlation of the GBMR (blue circles), where Δf is the RF spectral shift. By injecting NH_3 with the concentration ranging from 0 to 20 ppm, $|\Delta f|$ increases by 2.75 MHz correspondingly. Because of small volume of the GBMR, the rGO film with the surface area less than 2.5×10^4 μm^2 tends to be saturated at a relatively high NH_3 concentration. Hence the NH_3 concentration versus Δf correlation is not linear. However, when NH_3 concentration is below 5 ppm, it could be regarded as linear with an estimated sensitivity of 200 ± 0.2 kHz/ppm. In comparison, the red diamonds show the response of the similar order mechanical mode in a BMR without inner rGO film. Measured spectra of the BMR are shown in Supplementary Figure S7. In the BMR, there is no NH_3−graphene adsorption induced electron−phonon interaction and hence the F-SBS generated mechanical mode in the BMR shows almost no response to NH_3. Figure 3c plots the regeneration of the GBMR by launching NH_3 and dry air in periodically with concentration 1, 2, and 5 ppm, respectively. Determined by the gas injecting speed, the response takes several seconds. Measured results demonstrate that the GBMR has good recoverability (>90%), benefiting from the fast "on−off" process of the gas molecules−graphene adsorption. We also illustrate the response time of the GBMR sensor here. Along with NH_3 gas injection (fixed flow rate 1 nL/min), $|\Delta f|$ increases rapidly. By zooming the time scale in, Figure 3d plots the response and recovery curves of the GBMR sensor in details. The full width at half-maximum delay ($t_{1/2}$) is an average of 15−18 s for NH_3 gas response, whereas at 18−30 s for the recovery; such a fast response is useful for online monitoring.

In order to estimate the detection limit of the GBMR accurately, it is worth characterizing its maximum resolution. Maximum sampling resolution of our RF analyzer is 1 Hz, however the resolution is limited by the line width of the beat note, uncertainty of the mechanical mode, and the phase noise of the pump laser. Figure 4a zooms in on the Brillouin−acoustic mechanical modes beat note, where its Lorentzian-fitted spectral maximum is shifted by ±200 Hz. For a smaller spectral shift, it is difficult to characterize and hence we define the resolution R_F to be 200 Hz. In addition, by sampling 10 points for each gas concentration, Figure 4b plots the Allen deviation to estimate the spectral instability of the beat note, during gas detection. For gas concentration smaller than 10 ppm, the uncertainty induced by gas flow, laser drifting, and thermal noise is typically smaller than 200 Hz (by controlling the temperature more accurately, this result could be further improved). Considering the sensitivity shown in Figure 3 as 200 ± 0.2 kHz/ppm, the detection limit of this GBMR reaches 1 ppb. When gas concentration over 100 ppm, it has a maximum uncertainty up to 300 Hz.

Figure 4c illustrates the dynamic range of the GBMR. It is known that graphene-based gas sensors tend to be saturated when gas concentration is too high, determined by the effective surface area of the graphene. Once all surface sites of graphene are filled, further spectral shift would be too small to detect. As illustrated in Figure 4c, the correlation of sensitivity decreases exponentially with concentration. When the NH_3 concentration is higher than 450 ppm, the sensitivity is lower than 200 Hz/ppm, as the blue dots show. Meanwhile, considering the influence of the frequency uncertainty, we estimate that once the NH_3 concentration is higher than 370 ppm, the RF shift cannot be detected stably. That means to detect NH_3 gas with sub-ppm sensitivity, the dynamic range is up to 370 ppm, comparable to prior graphene-based gas sensors with detection range from tens of ppm to thousands of ppm.[18] Consequently, for our ppb detection limit our dynamic range is over 5 orders of magnitude.

In the above demonstrations, we mostly focus on the selected mechanical mode with order $N_M = 24$ and $f_M = 262$ MHz. Actually, in the GBMR there are multiple excitable mechanical modes satisfying both the phase-matching condition of the F-SBS and the FSRs of the resonator. By carefully tuning the pump frequency, we also generated other mechanical modes, such as modes with $f_M = 103$ MHz ($N_M = 10$) and $f_M = 775$ MHz ($N_M = 57$). Referring to eq 1, the sensitivity (S) of the GBMR is proportional to its momentum

$$S = \frac{\partial f_s}{\partial x} = \frac{2\pi n_s - 2\pi n_p}{(c - 2\pi v_A n_s)^2} \frac{\partial v_A}{\partial x} f_p \tag{2}$$

Here x is the gas concentration, v_A is the acoustic velocity of an acoustic mode, and each generated mechanical mode corresponds to a specific n_s. According to eq 2, for a fixed n_p and f_p, a smaller n_s brings higher sensitivity. It indicates that a higher-order mode is helpful for the sensitivity enhancement. On the other hand, $S \propto f_p$, and this means for a pair of specific mode-to-mode phase matching a higher frequency pump can also achieve a higher sensitivity. Figure 4d,e illustrates several measured sensitivities, by using different optomechanical modes, which are generated by tuning f_p. Besides the mechanical mode with resonant frequency 262 MHz, when tuning f_p to 190.5, 192.1, 192.6, and 194.8 THz, mechanical modes with $f_M \approx 103$, 76, 297, and 775 MHz are observed. In gas sensing, they have varied sensitivities, as shown in Figure 4e. Among them, our selected 262 MHz mode has the highest sensitivity. In practice, the mechanical modes also have different resonance Q-factor, noise, and surface deformation,[28] which would influence the sensing dynamics as well. Hence, for the gas detection by using a GBMR photon−phonon matching condition could be further optimized. Benefiting from its optical measuring method similar to fiber Bragg gratings (FBGs)[29], in applications the resonant modes are easy to characterize with the potential for networking for distributed sensing in the future.

In the last one, based on the 262 MHz mode, we also compare the maximum sensitivity when the GBMR sensor detecting varied gas molecules, as Figure 4f demonstrates. Determined by the adsorption nature of graphene material, the GBMR shows it highly selective to polar molecules, that is, ammonia (≈200 kHz/ppm), acetone (≈160 kHz/ppm), water vapor (≈120 kHz/ppm), and ethanol (≈110 kHz/ppm), whereas it has a much lower sensitivity to nonpolar molecules, that is, p-xylene (≈20 kHz/ppm, due to condensation), and

DOI: 10.1021/acs.nanolett.7b02176
Nano Lett. 2017, 17, 4996−5002

hydrogen (<5 kHz/ppm). We also note that the detection recovery of a high boiling point gas like acetone, ethanol, and *p*-xylene takes a much longer time (up to minutes), hence this sensor is most appropriate to perform as an ammonia gas detector. This property is also helpful for broadening its future potential in applications like gas chromatography.[17]

In summary, leveraging unique properties of the reduced graphene oxide nanosheet, we build a bridge between Brillouin optomechanics and gas molecular adsorptions. In the graphene-enhanced Brillouin optomechanical microresonator demonstrated, we expand electron−photon interaction in conventional graphene based optical sensors to electron−phonon−photon interaction, realizing a new platform for ultrasensitive and fast ammonia gas sensing with a noise equivalent limit down to 1 ppb and a wide dynamic range over five orders-of-magnitude. Moreover, such a graphene inner-coated high-*Q* WGM resonator also paves the way for designing new graphene-based optical cavities, which have wide potential in applications like plasmonics,[30] optofluidics,[31] and optomechanical manipulations.[32]

■ ASSOCIATED CONTENT

Supporting Information

The Supporting Information is available free of charge on the ACS Publications website at DOI: 10.1021/acs.nanolett.7b02176.

Detailed information on the theoretical analysis, fabrication of the graphene inner-deposited microresonator, measurement of optical *Q*-factors, experimental setup, and preparation of the gas samples. Measured results of NH_3 detection without rGO film and instability of the GBMR (PDF)

■ AUTHOR INFORMATION

Corresponding Authors

*E-mail: (B.Y.) by252@cam.ac.uk.
*E-mail: (Y.R.) yjrao@uestc.edu.cn.

ORCID

Baicheng Yao: 0000-0001-8368-5815
Yuanfu Chen: 0000-0002-6561-1684
Xudong Fan: 0000-0003-0149-1326

Author Contributions

B.Y. designed this work, Y.R. supported this work. B.Y., B.Y., C.B.Y., and H.W. performed the experiment. Y.W. contributed the gas sensing analysis, Y.G. helped the WGM resonance generation. Y.C. and Y.L. provided the graphene material used and helped its characterizations. B.Y., S.W.H., and X.F. performed the theoretical analysis. B.Y., C.W.W., X.F., and Y.R. prepared the manuscript.

Notes

The authors declare no competing financial interest.

■ ACKNOWLEDGMENTS

The authors thank instruments provided by Professor B. J. Wu and Dr. H. Zhou and helpful discussions with Professor Z. D. Xie and Dr. Y. J. Huang. This work is supported by the 111 project (B14039) and National Natural Science Foundation of China under Grants 61290312, 61475032, and 61575039, the Graphene Flagship of EU, and the National Science Foundation (U.S.A.) under Grant 1611598.3

■ REFERENCES

(1) Novoselov, K.; Geim, A.; Morozov, S.; Jiang, D.; Zhang, Y.; Dubonos, S.; Grigorieva, I.; Firsov, A. Electric field effect in atomically thin carbon films. *Science* **2004**, *306*, 666−669.
(2) Novoselov, K.; Geim, A.; Morozov, S.; Jiang, D.; Katsnelson, M.; Grigorieva, I.; Dubonos, S.; Firsov, A. Two-dimensional gas of massless Dirac fermions in graphene. *Nature* **2005**, *438*, 197−200.
(3) Liu, M.; Yin, X.; Avila, E.; Geng, B.; Zentgraf, T.; Zhang, X. A graphene-based broadband optical modulator. *Nature* **2011**, *474*, 64−67.
(4) Liu, M.; Yin, X.; Zhang, X. Double-Layer Graphene Optical Modulator. *Nano Lett.* **2012**, *12*, 1482−1485.
(5) Phare, C.; Lee, Y.; Cardenas, J.; Lipson, M. Graphene electro-optic modulator with30 GHz bandwidth. *Nat. Photonics* **2015**, *9*, 511−514.
(6) Martinez, A.; Sun, Z. Nanotube and graphene saturable absorbers for fibre lasers. *Nat. Photonics* **2013**, *7*, 842−845.
(7) Koppens, F.; Mueller, T.; Avouris, P.; Ferrari, A.; Vitiello, M.; Polini, M. Photodetectors based on graphene, other two-dimensional materials and hybrid systems. *Nat. Nanotechnol.* **2014**, *9*, 780−793.
(8) Singh, V.; Bosman, S.; Schneider, B.; Blanter, Y.; Castellanos-Gomez, A.; Steele, G. Optomechanical coupling between a multilayer graphene mechanical resonator and a superconducting microwave cavity. *Nat. Nanotechnol.* **2014**, *9*, 820−824.
(9) De Alba, R.; Massel, F.; Storch, I.; Abhilash, T.; Hui, A.; McEuen, P.; Craighead, H.; Parpia, J. Tunable phonon-cavity coupling in graphene membranes. *Nat. Nanotechnol.* **2016**, *11*, 741−746.
(10) Weber, P.; Güttinger, J.; Noury, A.; Vergara-Cruz, J.; Bachtold, A. Force sensitivity of multilayer graphene optomechanical devices. *Nat. Commun.* **2016**, *7*, 12496.
(11) Barton, R.; Storch, I.; Adiga, V.; Sakakibara, R.; Cipriany, B.; Ilic, B.; Wang, S. P.; Ong, P.; McEuen, P.; Parpia, J.; Craighead, H. Photothermal self-oscillation and laser cooling of graphene optomechanical systems. *Nano Lett.* **2012**, *12*, 4681−4686.
(12) Liu, Y.; Dong, X.; Chen, P. Biological and chemical sensors based on graphene materials. *Chem. Soc. Rev.* **2012**, *41*, 2283−2307.
(13) Xing, F.; Meng, G.; Zhang, Q.; Pan, L.; Wang, P.; Liu, Z.; Jiang, W.; Chen, Y.; Tian, J. Ultrasensitive flow sensing of a single cell using graphene-based optical sensors. *Nano Lett.* **2014**, *14*, 3563−3569.
(14) Rodrigo, D.; Limaj, O.; Janner, D.; Etezadi, D.; Abajo, F.; Pruneri, V.; Altug, H. Mid-infrared plasmonic biosensing with graphene. *Science* **2015**, *349*, 165−168.
(15) Schedin, F.; Geim, A.; Morozov, S.; Hill, E.; Blake, P.; Katsenlson, M.; Novoselov, K. Detection of individual gas molecules adsorbed on graphene. *Nat. Mater.* **2007**, *6*, 652−655.
(16) Dan, Y.; Lu, Y.; Kybert, N.; Luo, Z.; Johnson, A. Intrinsic response of graphene vapor sensors. *Nano Lett.* **2009**, *9*, 1472−1475.
(17) Kulkarni, G.; Reddy, K.; Zhong, Z.; Fan, X. Graphene nanoelectronic heterodyne sensor for rapid and sensitive vapour detection. *Nat. Commun.* **2014**, *5*, 4376.
(18) Shivananju, B.; Yu, W.; Liu, Y.; Zhang, Y.; Lin, B.; Li, S.; Bao, Q. The roadmap of graphene-based optical biochemical sensors. *Adv. Funct. Mater.* **2017**, *27*, 1616.
(19) Bahl, G.; Zehnpfennig, J.; Tomes, M.; Carmon, T. Stimulated optomechanical excitation of surface acoustic waves in a microdevice. *Nat. Commun.* **2011**, *2*, 403.
(20) Bahl, G.; Kim, K.; Lee, W.; Liu, J.; Fan, X.; Carmon, T. Brillouin cavity optomechanics with microfluidic devices. *Nat. Commun.* **2013**, *4*, 1994.
(21) Shen, Z.; Zhang, Y.; Chen, Y.; Zou, C.; Xiao, Y.; Zou, X.; Sun, F.; Guo, G.; Dong, C. Experimental realization of optomechanically induced non-reciprocity. *Nat. Photonics* **2016**, *10*, 657−662.
(22) Lopez-Polin, G.; Gomez-Navarro, C.; Parente, V.; Guinea, F.; Katsnelson, M.; Perez-Murano, F.; Gomez-Herrero, J. Increasing the elastic modulus of graphene by controlled defect creation. *Nat. Phys.* **2014**, *11*, 26−31.
(23) Yu, S.; Sun, X.; Ni, X.; Wang, Q.; Yan, X.; He, C.; Liu, X.; Feng, L.; Lu, M.; Chen, Y. Surface phononic graphene. *Nat. Mater.* **2016**, *15*, 1243−1247.

DOI: 10.1021/acs.nanolett.7b02176
Nano Lett. 2017, 17, 4996−5002

(24) Eda, G.; Fanchini, G.; Chhowalla, M. Large-area ultrathin films of reduced graphene oxide as a transparent and flexible electronic material. *Nat. Nanotechnol.* **2008**, *3*, 270−274.
(25) Yao, B.; Wu, Y.; Yu, C.; He, J.; Rao, Y.; Gong, Y.; Fu, F.; Chen, Y.; Li, Y. Partially reduced graphene oxide based FRET on fiber-optic interferometer for biochemical detection. *Sci. Rep.* **2016**, *6*, 23706.
(26) Zhu, J.; Ozdemir, S.; Xiao, Y.; Li, L.; He, L.; Chen, D.; Yang, L. On-chip single nanoparticle detection and sizing by mode splitting in an ultrahigh-Q microresonator. *Nat. Photonics* **2010**, *4*, 46−49.
(27) Yariv, A. Critical coupling and its control in optical waveguide-ring resonator systems. IEEE Photon. *IEEE Photonics Technol. Lett.* **2002**, *14*, 483−485.
(28) Lee, W.; Sun, Y.; Li, H.; Reddy, K.; Sumetsky, M.; Fan, X. A quasi-droplet optofluidic ring resonator laser using a microbubble. *Appl. Phys. Lett.* **2011**, *99*, 091102.
(29) Rao, Y. In-fibre Bragg grating sensors. *Meas. Sci. Technol.* **1997**, *8*, 355−377.
(30) Koppens, F.; Chang, D.; Abajo, F. graphene plasmonics: a platform for strong light−matter interactions. *Nano Lett.* **2011**, *11*, 3370−3377.
(31) Fan, X.; White, I. Optofluidic microsystems for chemical and biological analysis. *Nat. Photonics* **2011**, *5*, 591−597.
(32) Aspelmeyer, M.; Kippenberg, T.; Marquardt, F. Cavity optomechanics. *Rev. Mod. Phys.* **2014**, *86*, 1391.

DOI: 10.1021/acs.nanolett.7b02176
Nano Lett. 2017, 17, 4996−5002